Pulse inversion enhances the passive mapping of microbubble-based ultrasound therapy

Antonios N. Pouliopoulos, Mark T. Burgess, and Elisa E. Konofagou

Citation: Appl. Phys. Lett. **113**, 044102 (2018); doi: 10.1063/1.5036516
View online: https://doi.org/10.1063/1.5036516
View Table of Contents: http://aip.scitation.org/toc/apl/113/4
Published by the American Institute of Physics

Pulse inversion enhances the passive mapping of microbubble-based ultrasound therapy

Antonios N. Pouliopoulos,[1] Mark T. Burgess,[1] and Elisa E. Konofagou[1,2,a)]
[1]*Department of Biomedical Engineering, Columbia University, New York City, New York 10032, USA*
[2]*Department of Radiology, Columbia University, New York City, New York 10032, USA*

(Received 16 April 2018; accepted 6 July 2018; published online 24 July 2018)

Therapeutic ultrasound combined with preformed circulating microbubbles has enabled non-invasive and targeted drug delivery into the brain, tumors, and blood clots. Monitoring the microbubble activity is essential for the success of such therapies; however, skull and tissues limit our ability to detect low acoustic signals. Here, we show that by emitting consecutive therapeutic pulses of inverse polarity, the sensitivity in the detection of weak bubble acoustic signals during blood-brain barrier opening is enhanced compared to therapeutic pulses of the same polarity. Synchronous passive mapping of the cavitation activity was conducted using delay-and-sum beamforming with absolute time delays, which offers superior spatial resolution compared to the existing asynchronous passive imaging techniques. Sonication with pulse inversion allowed filter-free suppression of the tissue signals by up to 8 dB in a tissue-mimicking phantom and by 7 dB *in vivo,* compared to exposure without pulse inversion, enabling enhanced passive mapping of microbubble activity. Both therapeutic schemes resulted in similar free-field microbubble activation *in vitro* and efficient blood-brain barrier opening *in vivo*. *Published by AIP Publishing*. https://doi.org/10.1063/1.5036516

Microbubble-based focused ultrasound therapies provide a minimally invasive method to deliver drugs into tissues, tumors, blood clots, and individual cells. Microbubbles are routinely used in clinical ultrasound imaging as contrast agents and are currently being investigated as intravascular stress sources to induce therapeutic bioeffects.[1] When exposed to the alternating phases of an ultrasound field, they respond by expanding and contracting. These volumetric oscillations, known as acoustic cavitation, can be harnessed to achieve a desired therapeutic effect, such as targeted and non-invasive opening of the blood-brain barrier (BBB).[2] Due to the mechanical interaction between the oscillating microbubbles and the surrounding microvasculature,[3,4] the BBB has been shown to safely and reversibly open in a targeted area of the brain.

A defining factor determining the efficacy, safety, and reversibility of BBB opening is the selected therapeutic pulse shape and sequence, which affects the magnitude and distribution of induced stresses in the brain microvasculature. Although ms-long pulses have been primarily used to transiently open the BBB to date, μs-long pulses emitted at kHz pulse repetition frequencies (PRFs) were also shown to result in high drug delivery rates within the targeted brain region.[5] Such rapid short pulses have been shown to produce more uniform cavitation activity within the focal volume *in vitro*,[6,7] while reducing microbubble interactions, acoustic radiation forces, and clustering formation observed during ms-long sonication.[7–9]

Regardless of the therapeutic design, a major advantage of microbubble-based ultrasound therapies is the ability to passively monitor their evolution and capability of inducing a bioeffect in real-time. Passive cavitation detection (PCD) provides information about cavitation magnitude, duration, and mode,[6,10] but also the velocity of cavitation nuclei exposed to radiation forces.[11] PCD can be performed using two separate co-aligned transducers[6,11] or a single transducer.[12] Using linear or hemispherical arrays, one can localize the spatial location of the acoustic sources to perform cavitation mapping during therapy.[7,13,14] Passive imaging techniques can be used to monitor ultrasound therapies at arbitrary pulse lengths; however, their axial resolution remains poor despite recent advances.[15–17]

Short-pulse therapies combine the advantages of both therapeutic and imaging regimes, allowing active imaging concepts to be incorporated into the passive monitoring of therapeutic processes.[14] Burgess *et al*. implemented passive imaging with short therapeutic pulses to limit the duration of microbubble emissions. By synchronizing the emission and acquisition processes to acquire absolute time-of-flight information, delay-and-sum beamforming can be used to achieve superior resolution compared to existing passive techniques.[18] High-frequency probes can detect broadband emissions and localize the microbubble positions at high resolution, while avoiding interference from the primary acoustic field. However, interference between cavitation and tissue signals may arise when the therapeutic and imaging spectra overlap. Additionally, high-frequency probes are not appropriate for clinical applications due to the presence of the thick human skull, which hinders deep imaging and significantly attenuates acoustic signals of frequencies higher than 1–2 MHz. High-pass filtering can suppress signals originating from the skull, tissues, and slow-moving scatterers, when using overlapping frequencies. Filtering may significantly reduce the detected microbubble signal at frequencies below 1–2 MHz, which is the spectral region that can be more easily detected through a thick human skull. Furthermore, low sensitivity in detecting weak cavitation emissions is expected to be an important limitation in detection systems with limited dynamic range.

a)Author to whom correspondence should be addressed: ek2191@columbia.edu

A limiting factor for performing cavitation imaging through the skull is thus the contrast-to-tissue ratio (CTR). Although strong broadband signals produced by inertial cavitation can be transcranially detected using PCD,[19,20] weaker harmonic signals produced by microbubbles exposed to low-pressure ultrasound may be more difficult to detect through the thick skull of primates.[21] Furthermore, mapping of such signals during therapeutic ultrasound exposure is exacerbated by skull-induced aberrations, which distort the apparent position of acoustic events in the brain,[22] and by standing waves formed during long-pulse low-frequency sonication.[23]

To address these limitations and increase the CTR during monitoring of low-power BBB opening, we thereby propose an alternative short-pulse therapeutic design. Drawing inspiration from contrast-enhanced ultrasound imaging[24] and previous work on active monitoring of lesion formation during high-intensity focused ultrasound (HIFU) treatment,[25] we hypothesized that consecutive short therapeutic pulses of inverse polarity would increase the sensitivity of a given passive imaging system in detecting weak acoustic signals from within the brain. To test our hypothesis, we used passive imaging with delay-and-sum beamforming, which provides axial resolution comparable to B-mode imaging.[18] Therapeutic ultrasound with pulse inversion (PI) was expected to provide better CTR when compared to exposure with pulses of same polarity, by suppressing the acoustic signals emanating from linear scatterers such as the skull and tissues. Our aim was to compare the two therapeutic designs both *in vitro* and *in vivo* and investigate their differences in terms of BBB opening monitoring and drug delivery efficiency.

In vitro and *in vivo* experiments were conducted using the same experimental setup (Fig. 1). A single-element spherically focused 0.5 MHz ultrasound transducer (part number: H-204; Sonic Concepts, Bothell, WA, USA) was used to sonicate microbubbles in three different targets: (1) microbubbles circulating in free field within a water container; (2) microbubbles infused into a wall-less channel in a tissue-mimicking phantom filled with linear scatterers in its lower part [Figs. 1(a) and 3] microbubbles circulating in the murine vasculature *in vivo*. Two function generators (33500B Series, Agilent technologies, Santa Clara, CA, USA) produced the therapeutic pulse sequences. A short pulse [Fig. 1(b)-top] was emitted by the first function generator at a pulse repetition frequency (PRF) of 2 kHz. The following short pulse was emitted by the second function generator with a fixed delay of 250 μs. The second function generator produced a pulse with either positive or negative polarity. The acoustic waveforms at the focus of the therapeutic transducer were measured using a hydrophone, for pulses of both 0° [Fig. 1(b)-top] and 180° [Fig. 1(b)-center] phase. The sum of the inverse pulses had a normalized amplitude reduced by 97% or 30 dB compared to the free-field amplitudes of the original pulses [Fig. 1(b)-bottom], due to the suppression of the fundamental and odd harmonics in the summed signal (supplementary material, Fig. 1). The strong odd harmonics were mainly produced due to the high transmit transfer function of the therapeutic transducer at these frequencies,[12] following the application of a broadband single-cycle voltage pulse, and partially due to non-linear ultrasound propagation.

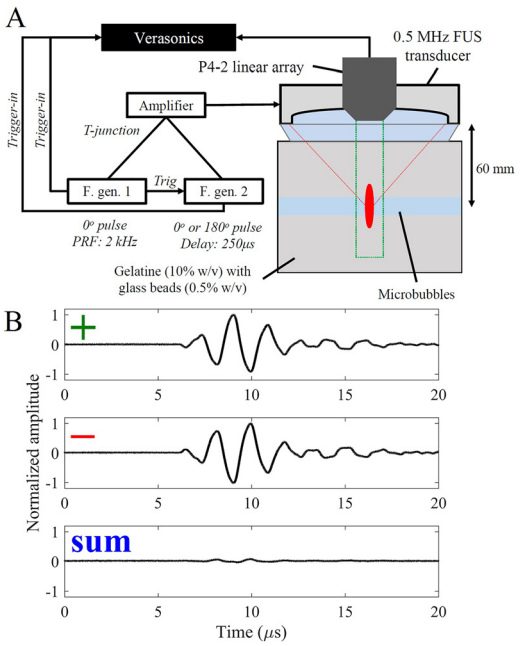

FIG. 1. Ultrasonic pulse inversion therapy method. (a) Experimental setup. A 0.5-MHz focused ultrasound transducer was used to sonicate microbubbles suspended in a bath, a tissue-mimicking phantom (shown here) or the murine brain. An inserted and co-aligned P4-2 array captured the emitted microbubble signal. Synchronous acquisition by the Verasonics research platform was triggered by two synchronized function generators, which emitted pulses of inverse polarity at a pulse repetition frequency of 4 kHz. (b) Pulse inversion principle. Pulses of positive and negative polarity were emitted through the therapeutic 0.5-MHz focused ultrasound transducer. Summation of their free-field waveforms in the time domain led to a signal cancellation of up to 30 dB.

In our previous work,[18] we used a high-frequency array (L22-14v) with a −6 dB bandwidth between 12.6 and 24.8 MHz. This frequency range was higher than the therapeutic frequency (i.e., 1 MHz), enabling isolation of the broadband microbubble signal from reflections at low frequencies. Although this array is ideal for small-animal studies, it is not applicable in large animals or humans, due to the thicker skull and larger imaging depths. Here, a P4-2 sector array (Philips Healthcare, Bothell, WA, USA) passively detected acoustic signals from the sonicated microbubbles in synchrony with the emitted pulses. A Verasonics Vantage research platform (Verasonics, Inc., Kirkland, WA, USA) was used to record and reconstruct the radio frequency (RF) data. RF acquisition was initiated 6 μs after the pulse emission, to account for the time of flight between the therapeutic transducer and the passive imaging array. Synchronizing emission and reception provided absolute time-of-flight information. Following the method described by Burgess *et al.*,[18] we constructed power cavitation maps that indicated the distribution and mean intensity of acoustic cavitation activity within the focal area. To harvest the effect of PI, we accumulated the in-phase quadrature (IQ) data of consecutive pulses of inverse polarity and averaged RF data from 10 pulse pairs to construct a single frame. A total of 100 frames were used to construct power cavitation maps, by accumulating the image intensity of all frames. Following in-line IQ averaging and summation of the 100 frames, the

effective frame rate of cavitation mapping was 0.2 Hz. All maps were normalized to the exposure without PI to account for signal reduction due to the PI effect and allow for comparison. To quantify the CTR, we measured the mean intensity in two regions of interest (ROIs), corresponding to tissue and bubble signal, respectively. We have also tested the suppression efficiency using asynchronous passive acoustic mapping (PAM),[13] to investigate the applicability of therapy with PI in different passive imaging algorithms. Details of the image reconstruction routine are given in Ref. 18.

In vivo experiments evaluated the effect of PI in terms of microbubble detectability through the skull and the produced BBB opening. Ten wild-type mice (C57BL/6, mass: 21 ± 3 g, age: 4–6 weeks) were exposed to therapeutic sequences without (n = 5) or with (n = 5) PI [peak-negative pressure (PNP): 700 kPa, pulse length: 2.5 cycles or 5 μs, PRF: 4 kHz, duty cycle: 2%, sonication duration: 2.5 min]. Mice were anesthetized using isoflurane (2%–3%) mixed with oxygen and were maintained under anesthesia (1%–1.5%) throughout the experimental procedures. A control sonication was performed to acquire a baseline signal and measure the reduction in the signal from linear scatterers with PI and without microbubbles. In-house manufactured polydisperse microbubbles (diameter: 1.37 ± 1.02 μm, lipid shell composition: DSPC and DSPE-PEG2000 at molar ratio of 9:1) were then infused as a bolus through the tail vein. Approximately 2×10^7 microbubbles per ml of blood were introduced into circulation, which was equivalent to 10× the clinical dose approved for ultrasound imaging applications. In our previous work,[18] size-isolated 4–5 μm microbubbles were used to perform cavitation mapping and BBB opening *in vivo*. However, commercially available microbubbles are polydisperse, so here we chose to work with polydisperse populations to enhance our clinical relevance.

Following sonication, 200 μl of gadolinium(Gd)-based MRI contrast agent was injected intraperitoneally. T_1-weighted MR sequences were acquired in a small-animal 9.4 T MRI system to confirm BBB opening and investigate Gd diffusion into the brain parenchyma.

All data are presented as mean ± s.d. (n = 10 for *in vitro* and n = 5 for *in vivo* experiments). To evaluate statistically significant differences, we performed either parametric paired t-tests or non-parametric Wilcoxon Rank tests, depending on the normality of the data (assessed with a two-sample F-test). Statistical significance was assumed at $p < 0.05$.

To determine microbubble activation and detection sensitivity in free field, therapeutic sequences with and without PI were applied in a water tank filled with cavitation nuclei (10^6 microbubbles per ml). Microbubble emissions were detected throughout the focal volume for both sequences [Figs. 2(a) and 2(b)]. Due to the PI effect, the total microbubble signal from within the focal area during PI exposure [Fig. 2(b)] was suppressed compared to sonication without PI [Fig. 2(a)]. Although the cumulative intensity was reduced, the activation patterns were similar for both therapeutic designs throughout the acoustic pressures tested. Gaussian fits were applied along the axial and lateral dimensions (supplementary material, Fig. 2) to determine the size

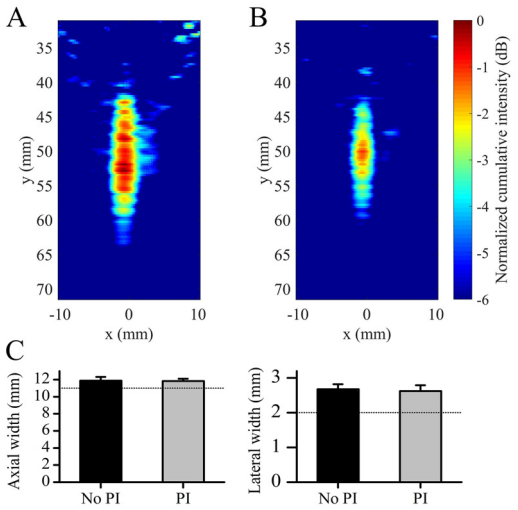

FIG. 2. Microbubble activation in free field does not depend on the polarity difference between pulses. Consecutive pulses of same (a) and inverse (b) polarity produced equivalent cumulative cavitation images in free field. Bubble signal was suppressed by 2 dB in PI compared to no PI (PNP: 700 kPa). (c) Axial (left) and lateral (right) widths of the apparent focal volume. There was no significant difference ($p > 0.05$) between PI and no PI for both the axial and lateral beam widths. Dotted line represents the nominal −3 dB beam widths along the axial and lateral dimensions, respectively. Data are presented as mean ± standard deviation (n = 10).

of the activated area (inclusion criterion: $R^2 > 0.9$) and compare it to the focal size measured with a hydrophone.

Although normalization reduced the visible contour in Fig. 2(b), the axial and lateral FWHM of the apparent ellipsoidal activity were not significantly different ($p > 0.05$) between the two sequences [Fig. 2(c)]. Both axial [Fig. 2(c)-left] and lateral [Fig. 2(c)-right] widths were equal and moderately higher than the nominal −3 dB beam width along each dimension (dotted lines). Free-field experiments showed that there was no difference in the sensitivity in microbubble detection with and without PI, as expected. However, there was a considerable suppression of between 0.8 and 3.9 dB in the detected cavitation signal (supplementary material, Fig. 3). The effect of PI was observed for pulses of arbitrary pulse length (e.g., 50 cycles, supplementary material, Fig. 4) and was similar between synchronous and asynchronous passive imaging techniques (supplementary material, Fig. 5), providing evidence that PI can improve the monitoring of any low-power therapeutic ultrasound application with a given passive imaging system.

Our hypothesis in this study was that PI would increase the CTR by suppressing signals originating from linear scatterers. To test this hypothesis, microbubbles infused into a wall-free channel [white lines in Fig. 3(a)] of a tissue-mimicking phantom were exposed to therapeutic sequences with and without PI at the absence of flow. Glass beads (size: 40–75 μm) were embedded within the gelatin and acted as linear scatterers within the therapeutic beam. Signals from glass beads were detected during excitation without PI [Fig. 3(a)]. However, this signal was significantly suppressed during PI exposure [Fig. 3(b)].

To quantify the differences in CTR, we isolated two ROIs within the phantom based on B-mode images (supplementary material, Fig. 6), corresponding to bubble and tissue areas, respectively. The measured CTR was consistently higher in PI

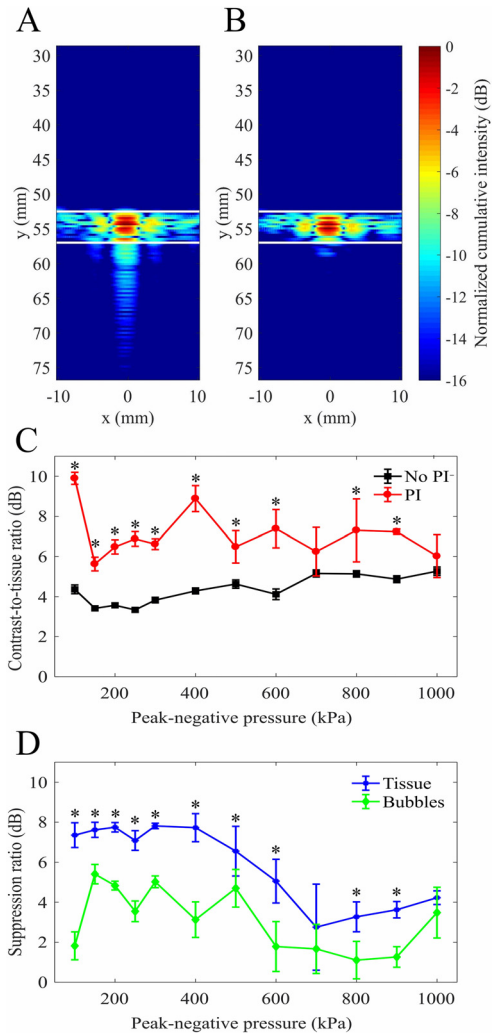

FIG. 3. PI increases the contrast-to-tissue ratio of cavitation mapping in a tissue-mimicking phantom. Cumulative intensity images of pulses of same (a) and inverse (b) polarity. Acoustic signals from linear scatterers within the ultrasound path are suppressed by PI (PNP: 100 kPa). (c) Contrast-to-tissue ratio was higher in PI (red circles) that no PI (black squares) at all the acoustic pressures tested. (d) Suppression ratios of tissue signals (blue crosses) were consistently higher than bubble signals (green diamonds) across the acoustic pressures. Data are presented as mean ± standard deviation (n = 10). *: $p < 0.05$.

exposure throughout the acoustic pressures which are relevant to BBB opening applications [Fig. 3(c)]. Using PI, the CTR increased by up to 5.5 dB at low acoustic pressures, which are preferable for safe and reversible BBB opening but difficult to produce detectable microbubble activity *in vivo*. The CTR range was 5.6–9.9 with PI and 3.3–5.3 without PI. The observed CTR increase stemmed from the difference in the suppression ratios between bubble and tissue signals [Fig. 3(d)]. Echoes from linear scatterers were more efficiently suppressed throughout the acoustic pressures. PI suppressed linear echoes by up to 7.8 dB at low acoustic pressures. The tissue suppression ratio ranged from 2.7 to 7.8 dB, while the bubble suppression ratio ranged from 1.1 to 5.4 dB. Both ratios followed a decreasing trend with pressures, indicating that PI is primarily effective in the low-power regime.

Non-linear ultrasound propagation was expected to be more pronounced at higher pressures, leading to an increase of the harmonic content of the therapeutic pulse, including an elevation of the second harmonic which is not suppressed by PI. Based on our data, the tissue suppression ratio was decreased at higher pressures [Fig. 2(d)]. This was expected to lead to a decrease of the CTR in PI [Fig. 2(c)]. Additionally, higher pressures trigger more violent microbubble collapses, i.e., stronger broadband component with a decrease in the harmonic amplitude.[11] We speculate that a decrease in the even harmonics would lead to a decrease in the produced CTR.

The position of the tissue ROI distal to the microbubble population may have resulted in a decrease of the acoustic pressure due to acoustic shielding effects. Furthermore, a pressure decrease was expected throughout the bubble and tissue ROI due to ultrasound attenuation, therefore the reported CTR values are an averaged approximation.

To test the potential of PI in BBB opening, we conducted a pilot *in vivo* study. Control sonications at the absence of microbubbles showed that signals from linear scatterers, such as the membrane, skull and tissues, were suppressed by 7 dB using PI [supplementary material, Figs. 7 and 8 (Multimedia view)]. Upon microbubble infusion, echoes originated from within the brain vasculature became readily apparent [supplementary material, Fig. 9 (Multimedia view)]. While skull and bubble signals appeared indistinguishable during sonication without PI, exposure with PI sequences resulted in clear separation between the suppressed skull echo and the bubble signals [Fig. 4(a) and supplementary material, Fig. 9 (Multimedia view)]. Delineation was possible due to the higher suppression in linear reflections compared to the bubble signals [Fig. 4(e)]. Contrast-enhanced MRI revealed that both sequences resulted in BBB opening in a mouse model [Figs. 4(c) and 4(d)]. Within our experimental groups (n = 5 per condition), there was no significant difference in the T_1 signal increase [Fig. 4(f)], indicating that the two therapeutic paradigms are equivalent in terms of drug delivery efficiency.

Monitoring of microbubble-mediated ultrasound therapies can be improved by appropriately designing the exposure scheme. Here, we designed and tested a therapeutic sequence building upon concepts of ultrasound imaging[24] and active monitoring of HIFU ablation.[25] Therapeutic PI sequences significantly increased the CTR compared to no-PI sequences (Fig. 3) without significant change of the therapeutic field (Fig. 2). Improved CTR facilitated monitoring of microbubble signals during BBB opening *in vivo*, allowing clear delineation of cavitation signals from linear scattering (Fig. 4).

Stationary signals from the skull and soft tissues can be eliminated by using a high-frequency linear array,[18] applying a high-pass filter or beamforming specific frequency bands.[14,16] Frequency-based passive cavitation imaging (PCI) is beneficial for fast mapping of isolated harmonic, ultraharmonic or broadband signals.[14,16,26,27] Although such information is useful in high-pressure and long-pulse therapies, low-pressure and short-pulse sequences used in BBB opening or targeted drug release require systems with sufficient dynamic range for efficient cavitation mapping. Furthermore, another limitation of existing passive techniques is the poor axial resolution (supplementary material, Fig. 5). For our system, the nominal axial resolution would be equal to 11.6 mm,[13] which is insufficient to distinguish between tissue and bubble responses in a phantom or *in vivo*. For this reason, we

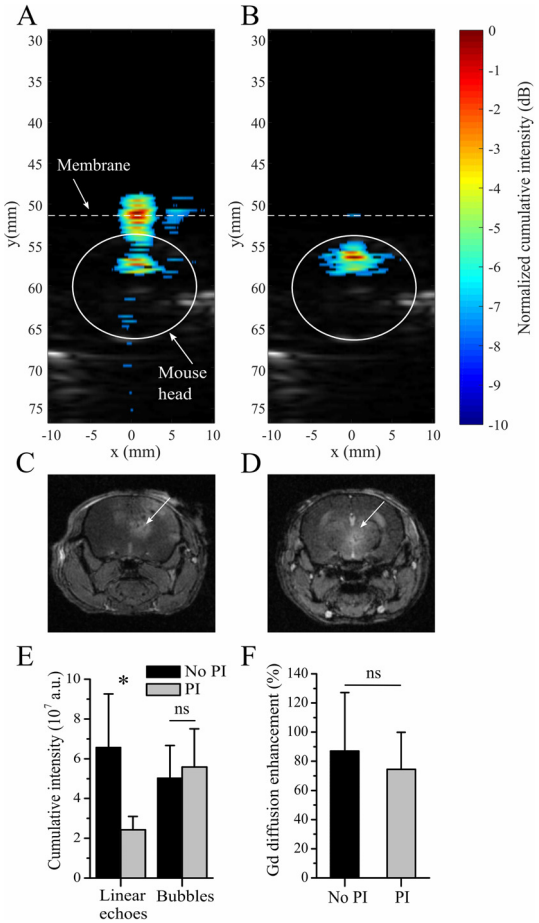

FIG. 4. PI facilitates microbubble signal mapping during blood-brain barrier opening in a mouse model. (a), (b) Cumulative acoustic maps during blood-brain barrier opening using consecutive pulses of same (a) and inverse (b) polarity (PNP: 700 kPa). PI suppressed echoes from linear scatterers. (c), (d) MRI scans of Gd perfusion into the brain parenchyma with (d) and without (c) PI. (e) Echoes originating from the linear scatterers were significantly lower with PI. Instead, bubble signal was non-significantly different with PI. (f) PI did not significantly change the delivered amount of Gd into the brain parenchyma. Data are presented as mean ± standard deviation (n = 5). *:$p < 0.05$.

calculated the CTR only using power cavitation imaging.[18] However, the PI sequence is expected to have similar suppression effects in both time-domain-based PAM[13,15,17] (supplementary material, Fig. 5) or frequency-domain-based PCI,[14,27–29] by exploiting the PI effect.

A limitation of our technique is that it can be used only for short-pulse microbubble-based ultrasound therapies, such as BBB opening, sonoporation, and ultrasound-triggered drug release. Other therapeutic applications such as HIFU ablation require thousands of ultrasound cycles,[29] which would deteriorate the axial resolution of the cavitation mapping (supplementary material, Fig. 4). Furthermore, the broadband frequency content of the microbubble emissions does not allow for meaningful spectral analysis.

In conclusion, we introduced a therapeutic ultrasound paradigm that may aid in monitoring low-pressure ultrasound therapies. PI increased the CTR by up to 5.5 dB compared to no PI and suppressed the tissue signals by 8 dB in a tissue-mimicking phantom. Ultrasonic therapy with PI suppressed the detected stationary signals by 7 dB *in vivo*, without significant reduction in the detected microbubble signal or the drug delivery efficiency.

See supplementary material for a theoretical analysis of the PI technique along with supplementary methods, figures, and multimedia files.

This study was funded by the NIH Grant Nos. 5R01EB009041 and 5R01AG038961. The authors acknowledge the members of the Ultrasound Elasticity Imaging Laboratory (UEIL) for their constructive input during the development of this technique. A.N.P. wishes to acknowledge Dr. Kirsten Christensen-Jeffries, Ms. Jemma Brown, and Ms. Sophie Morse for stimulating discussions.

[1]K. Ferrara, R. Pollard, and M. Borden, Annu. Rev. Biomed. Eng. **9**, 415 (2007).
[2]K. Hynynen, N. McDannold, N. Vykhodtseva, and F. A. Jolesz, Radiology **220**, 640 (2001).
[3]C. F. Caskey, D. E. Kruse, P. A. Dayton, T. K. Kitano, and K. W. Ferrara, Appl. Phys. Lett. **88**, 033902 (2006).
[4]H. Chen, A. A. Brayman, and T. J. Matula, Appl. Phys. Lett. **101**, 163704 (2012).
[5]J. J. Choi, K. Selert, F. Vlachos, A. Wong, and E. E. Konofagou, Proc. Natl. Acad. Sci. U.S.A. **108**, 16539 (2011).
[6]A. N. Pouliopoulos, S. Bonaccorsi, and J. J. Choi, Phys. Med. Biol. **59**, 6941 (2014).
[7]A. N. Pouliopoulos, C. Li, M. Tinguely, V. Garbin, M.-X. Tang, and J. J. Choi, J. Acoust. Soc. Am. **140**, 2469 (2016).
[8]H. Koruk, A. El Ghamrawy, A. N. Pouliopoulos, and J. J. Choi, Appl. Phys. Lett. **107**, 223701 (2015).
[9]C. Lazarus, A. N. Pouliopoulos, M. Tinguely, V. Garbin, and J. J. Choi, J. Acoust. Soc. Am. **142**, 3135 (2017).
[10]F. E. Shamout, A. N. Pouliopoulos, P. Lee, S. Bonaccorsi, L. Towhidi, R. Krams, and J. J. Choi, Ultrasound Med. Biol. **41**, 2435 (2015).
[11]A. N. Pouliopoulos and J. J. Choi, Phys. Med. Biol. **61**, 6154 (2016).
[12]S. V. Heymans, C. F. Martindale, A. Suler, A. N. Pouliopoulos, R. J. Dickinson, and J. J. Choi, IEEE Trans. Ultrason. Ferroelectr. Freq. Control **64**, 1234 (2017).
[13]M. Gyöngy and C.-C. Coussios, J. Acoust. Soc. Am. **128**, EL175 (2010).
[14]K. J. Haworth, T. D. Mast, K. Radhakrishnan, M. T. Burgess, J. a Kopechek, S.-L. Huang, D. D. McPherson, and C. K. Holland, J. Acoust. Soc. Am. **132**, 544 (2012).
[15]C. Coviello, R. Kozick, J. Choi, M. Gyöngy, C. Jensen, P. P. Smith, and C.-C. Coussios, J. Acoust. Soc. Am. **137**, 2573 (2015).
[16]C. Arvanitis, N. McDannold, and G. Clement, J. Acoust. Soc. Am. **138**, 1845 (2015).
[17]E. Lyka, C. Coviello, R. Kozick, and C.-C. Coussios, J. Acoust. Soc. Am. **140**, 741 (2016).
[18]M. T. Burgess, I. Apostolakis, and E. E. Konofagou, Phys. Med. Biol. **63**, 065009 (2018).
[19]Y. S. Tung, F. Marquet, T. Teichert, V. Ferrera, and E. E. Konofagou, Appl. Phys. Lett. **98**, 163704 (2011).
[20]C. D. Arvanitis, M. S. Livingstone, N. Vykhodtseva, and N. McDannold, PLoS One **7**, e45783 (2012).
[21]S.-Y. Wu, Y.-S. Tung, F. Marquet, M. Downs, C. Sanchez, C. Chen, V. Ferrera, and E. Konofagou, IEEE Trans. Ultrason. Ferroelectr. Freq. Control **61**, 966 (2014).
[22]R. M. Jones, M. A. O'Reilly, and K. Hynynen, Med. Phys. **42**, 4385 (2015).
[23]M. A. O'Reilly, Y. Huang, and K. Hynynen, Phys. Med. Biol. **55**, 5251 (2010).
[24]C.-C. Shen, Y.-H. Chou, and P.-C. Li, J. Med. Ultrasound **13**, 3 (2005).
[25]J. H. Song, Y. Yoo, T. K. Song, and J. H. Chang, Phys. Med. Biol. **58**, 5333 (2013).
[26]K. J. Haworth, K. B. Bader, K. T. Rich, C. K. Holland, and T. D. Mast, IEEE Trans. Ultrason. Ferroelectr. Freq. Control **64**, 177 (2017).
[27]C. D. Arvanitis, C. Crake, N. McDannold, and G. T. Clement, IEEE Trans. Med. Imaging **36**, 983 (2017).
[28]V. A. Salgaonkar, S. Datta, C. K. Holland, and T. D. Mast, J. Acoust. Soc. Am. **126**, 3071 (2009).
[29]K. J. Haworth, V. A. Salgaonkar, N. M. Corregan, C. K. Holland, and T. D. Mast, Ultrasound Med. Biol. **41**, 2420 (2015).